Varying proliferative and clonogenic potential in NRAS -mutated congenital melanocytic nevi according to size

Sarah Guégan, Natacha Kadlub, Arnaud Picard, Thomas Rouillé, Christelle Charbel, Aurore Coulomb-L'Hermine, Alexandre How-Kit, Sylvie Fraitag, Selim Aractingi, Romain H. Fontaine

Article type: regular article

Title: Varying proliferative and clonogenic potential in *NRAS*-mutated congenital melanocytic nevi according to size

Authors affiliations: Sarah Guégan[1,2,3], Natacha Kadlub[4,5], Arnaud Picard[4,5], Thomas Rouillé[1,2], Christelle Charbel[1,2], Aurore Coulomb-L'Hermine[2,6], Alexandre How-Kit[7], Sylvie Fraitag[8], Selim Aractingi[1,4,9,†], Romain H. Fontaine[1,2, †]

[1]Institut National de la Santé et de la Recherche Médicale (INSERM), U938, Saint-Antoine Research Center, 75012 Paris, France.

[2]Université Pierre et Marie Curie-Paris VI, 75005 Paris, France.

[3]Assistance Publique-Hôpitaux de Paris, Hôpital Tenon, Department of Dermatology, 75020 Paris, France.

[4]Université René Descartes-Paris V, 75005 Paris, France.

[5]Assistance Publique-Hôpitaux de Paris, Hôpital Necker-Enfants-Malades, Department of Maxillofacial and Plastic Surgery, 75015 Paris, France.

[6]Assistance Publique-Hôpitaux de Paris, Hôpital Trousseau, Department of Pathology, 75012 Paris, France.

[7]Laboratory for Functional Genomics, Fondation Jean Dausset – CEPH, Paris, France

[8]Assistance Publique-Hôpitaux de Paris, Hôpital Necker-Enfants-Malades, Department of Pathology, 75015 Paris, France.

[9]Assistance Publique-Hôpitaux de Paris, Hôpital Cochin, Department of Dermatology, 75014 Paris, France.

[†]Both authors contributed equally to this work as senior co-authors.

Corresponding author: Selim Aractingi, INSERM U938-UPMC, Saint-Antoine Research Center, 27 Rue de Chaligny, 75012 Paris, France.

Tel. Number: +33140011459

Fax number: +33140011423

E-mail: selim.aractingi@gmail.com

Word count : 3847

Display items : 4

Abbreviations: CMN: Congenital Melanocytic Nevus; DIV: Days *In Vitro*; lCMN: Large Congenital Melanocytic Nevus; mCMN: medium Congenital Melanocytic Nevus

ABSTRACT

Congenital melanocytic nevi (CMN) are benign proliferations that may be associated with various consequences depending on their size. They are characterized by a specific molecular signature, namely a post-zygotic somatic *NRAS* or *BRAF* mutation. We have recently reported that large CMN (lCMN), which are classically associated with an increased melanoma risk, harbor cell subpopulations with specific clonogenic and tumorigenic potential. We wished to ascertain whether cells displaying similar properties persisted postnatally in medium CMN (mCMN). Eighteen medium M1, nine large and one giant *NRAS*-mutated CMN were prospectively included in the study. Subpopulations of mCMN cells expressed stem cell/progenitor lineage markers such as Sox10, Nestin, and Oct4, as was the case in lCMN. Nevertheless, conversely to lCMN, mCMN cells with clonogenic properties were rarer. *In vitro*, approximatively 1 in 1500 cells isolated from fresh mCMN formed colonies that could be passaged. *In vivo*, mCMN seemed to harbor cells with less proliferative potential than the larger lesions as lCMN biopsies displayed a three-fold expansion compared to mCMN when xenografted in Rag2$^{-/-}$ mice. Thus, our data revealed variations in clonogenicity and tumorigenic properties in *NRAS*-mutated CMN according to size.

KEYWORDS

congenital melanocytic nevus, melanocyte, *NRAS* mutation, nevosphere, immunocompromised mice

INTRODUCTION

Congenital melanocytic nevi (CMN) are melanocytic proliferations of neural crest origin. Various clinical features such as body site, number of satellite lesions, color heterogeneity, surface rugosity, hypertrichosis and presence of nodules are of interest and have been integrated in the most recent classification used to describe these benign tumors (1). Nevertheless, the maximal size the nevus is expected to reach by adulthood i.e. projected adult size (PAS) remains a major criterion for CMN categorization. Small and medium CMN are characterized by a PAS respectively of less than 1.5 cm or between 1.5 and 20 cm. They are reported approximately in 1 in 100 births (2). Large CMN display a PAS from 20 cm to 40 cm and are rarer. They have an estimated prevalence of 1 in 20,000 to 1 in 50,000 births, giant CMN (PAS above 40 cm) of 1 in 200,000 to 1 in 500,000 births (3–6).

CMN result predominantly from a post-zygotic somatic *NRAS* or *BRAF* mutation (7–11). Nevertheless, molecular signature differs slightly depending on nevus size. In the vast majority of cases, an *NRAS* mutation is described in lCMN as reported in the most recent studies (8,9,12). In Kinsler et al. study analyzing 55 samples from 15 patients with multiple CMN with a PAS above 10 cm, all CMN were *NRAS*-mutated (8). In Charbel et al. study, an *NRAS* Q61 mutation was detected in 100% of CMN with a PAS above 20 cm (9). However, in Salgado et al. study that analyzed 66 prospectively collected CMN, 80.6% (29/36) of giant CMN and 80.0% (16/20) of large CMN harbored an *NRAS* Q61 mutation. Of note, 1/20 large CMN and 4/36 giant CMN (5% and 11.4% respectively) harbored a *BRAF* V600E mutation (12). On the other hand, small and medium CMN bear more frequently *BRAF* mutations. In Charbel et al. study, a *BRAF* V600E mutation was detected in 30% of small and medium M1 CMN (9). Nevertheless, other genetic alterations have recently been reported in these benign tumors. Kinsler and colleagues have shown that germline *MC1R* phenotype may alter CMN size and multiplicity (13).

Large CMN predispose to oncological as well as neurological complications. An overall 2% risk of melanoma transformation has recently been ascertained in these lesions (14,15). This risk is associated with lesion size and is particularly high in giant nevi (15); it is considered much lower in small CMN, probably similar to the one observed in acquired naevi. We have recently reported that *NRAS*-mutated lCMN harbor nevocytic cell subpopulations with persisting post-natal clonogenic and tumorigenic potential (16). These cells were growth-factor dependent, grew as *NRAS*-mutated nevospheres *in vitro* and could be passaged. Interestingly, another group has cultured *NRAS*-mutated cell populations isolated from 4 patients with neurocutaneous melanocytosis: these cells grew similarly as spheroid colonies *in vitro,* retained their genetic identity and were sensitive to drugs targeting the NRAS signaling pathway (17). As a difference in terms of transformation risk has been reported depending on CMN size, we speculated whether a difference in clonogenic and tumorigenic potential could correlate with nevus size. Thus, our aim was to better characterize nevocytic cells isolated from mCMN by assessing their nevosphere formation potential and tumorigenic properties as compared to lCMN.

METHODS

Study approval and subjects

The study was approved by the institutional independent ethics committee (Comité de Protection des Personnes Ile-de-France V) and complied with the Declaration of Helsinki Principles. The patients' guardians provided written informed consent before their participation. CMN were obtained from the plastic surgery department of Armand Trousseau and Necker-Enfants-Malades hospitals. Clinical phenotyping of patients was performed by SG and NK. Classification was done using the projected adult size (PAS) of the largest lesion.

Genotyping

DNA extraction was performed as previously described (9).

Standard real-time PCR. The detection of *NRAS* codons 61 and *BRAF* codon 600 mutations was performed by standard real-time PCR on a LightCycler 480 thermocycler (Roche Applied Science, Penzberg, Germany). 25 ng of genomic DNA were used as template in a 25 µL PCR mix including 1x HotStar Taq DNA polymerase Buffer, 1.6 mM of additional $MgCl_2$, 200 µM of dNTPs, 200 nM of each primer (for *NRAS*: GTTGGACATACTGGATAC and Biotin-ATGACTTGCTATTATTGATG and for *BRAF*: CCTTTACTTACTACACCTCAGATA and Biotin-GACAACTGTTCAAACTGATGGGA), 2 µM of SYTO9 and 2 U of HotStar Taq DNA polymerase. Initial denaturation step was performed at 95°C for 10 min, followed by 50 cycles of 20 sec denaturation at 95°C, 20 sec annealing at 55°C for *NRAS* assay and 62°C for *BRAF* assay and 10 sec elongation at 72°C. Mutation detection was performed subsequently by pyrosequencing with a limit of detection of 7% of the mutant allele.

E-ice-COLD-PCR. The sensitive detection of *NRAS* codons 61 and *BRAF* codon 600 mutations was performed by E-*ice*-COLD-PCR (18,19) using the same thermocycler and the same PCR mix conditions as described before, supplemented with 50 nM of *NRAS* blocker

probe (*NRAS*_BK_LNA GATACAGCTGGA+C+A+AGAAGAGTACAGTGCCATGAGAGACCAATACATGAG-Phosphate) or 100 nM of *BRAF* blocker probe (*BRAF*_BK_LNA ATGGGACCCACTCCATCGAGATTT+C+A+CTGTAGCTAGACCAAAATCACCTATTTTACTGTGAGG-Phosphate). An initial denaturation step was performed 10 min at 95°C, followed by 6 cycles of standard PCR (30 sec denaturation at 95°C, 20 sec annealing at 55°C for *NRAS* assay and 62°C for *BRAF* assay and 10 sec elongation at 72°C) and 44 cycles of E-*ice*-COLD-PCR [20 sec denaturation at 95°C, 30 sec blocker annealing at 70°C, 20 sec denaturation at critical temperature (78°C for *NRAS* assay and 76°C for *BRAF* assay), 20 sec primer annealing (55°C for *NRAS* assay and 62°C for *BRAF* assay) and 10 sec elongation at 72°C] to enrich the mutations. Mutation detection was performed subsequently by pyrosequencing with a limit of detection evaluated at 0.1% of the mutant allele (18,19).

Pyrosequencing. PCR products were purified and rendered single-stranded on a PyroMark-Q96 Vacuum Workstation (Qiagen, Hilden, Germany) and the mutation detection, identification and quantification were performed by genotyping on a PyroMark-Q96 MD pyrosequencer (Qiagen) using the following sequencing primers: TGGACATACTGGATACAGC for *NRAS* assay and GGTGATTTTGGTCTAGCTAC for *BRAF* assay (19,20).

Immunostainings

Paraffin-embedded CMN tissue sections were labeled with anti-human MITF (1:250), Nestin (1:100), KI67 (1:100), Oct4 (1:100), Melan-A (1:100) and Sox10 (1:100) (Detailed in Supplementary Methods).

In vitro assays

Fresh nevocytic cell suspensions deriving from patients were seeded at a density of 50000 cells per well in DMEM/F12 supplemented with EGF (100ng/mL), bFGF (100 ng/mL), B27 supplement and insulin (5 ug/mL). Nevospheres numbers were counted, and sphere diameters were measured. Number and frequency of initiating cells were determined using limiting dilution analysis (16,21) (Detailed in Supplementary Methods).

In vivo assays

Animals experiments were performed according to experimental protocols following European Community Council guidelines and approved by our Institutional Animal Care and Use Committee (approval number Ce5/2012/003). Full-thickness CMN punch biopsies of 3mm diameter and 3.5mm height were xenografted in brown adipose tissue in $Rag2^{-/-}$ mice as previously described (16). Xenografts were collected after 3 or 7 months. Xenografts diameter and height were measured with a caliper, and the grafted volume tumor was obtained as V= Width (w) x Length (l) x Height (h). Paraffin-embedded sections were stained with haematoxylin-eosin (TA-125-MH, Thermoscientific). Xenograft sections were also labeled with mouse anti-human mitochondria antibody Cy3 conjugated (Dilution 1:25, MAB1273C3, clone 113-1, Merck Millipore, Fontenay-sous-Bois, France).

Statistical analysis

The data were analyzed using Unpaired Student's t-test. For all results, n indicates the number of independent experiments performed. In all histograms, asterisks correspond to: *$p \leq 0.05$, **$p \leq 0.01$, ***$p \leq 0.001$.

Results

Clinical and genetic characteristics

Twenty-eight patients whose ages varied between 3 months and 16 years were prospectively included in the study. Of note, patients 19 to 23 were previously included in (16). Clinical characteristics are reported in Tables 1 and S1. Patients were subdivided in 2 groups: a medium M1 CMN group (mCMN) and a large CMN group (lCMN). The mCMN group was composed of 18 patients displaying medium M1 CMN defined by a PAS from 1.5 to 10 cm. The lCMN group comprised 9 patients with large CMN (PAS above 20 cm and up to 40 cm) and one patient with a giant CMN (PAS above 40 cm). Ages varied from 5 months to 16 years in the mCMN group (median age, 27.5 months) and from 3 months to 5 years in the lCMN group (median age, 8 months). lCMN were more associated with satellites and displayed more heterogeneity of color, rugosity, hairiness and nodules than mCMN (Table S1).

The *NRAS* exon 2 and 3 and *BRAF* exon 15 mutational status of the samples was ascertained using pyrosequencing and E-*ice*-COLD-PCR. All CMN were *NRAS*-mutated and did not harbor any *BRAF* mutation (Table 1).

Both mCMN and lCMN cells display progenitor/stem cell markers

Firstly, mCMN and lCMN were compared using various immunohistochemical stainings (Fig. 1). Melanocytic markers such as Melan-A (Fig. 1a) and MITF (Fig. 1b) revealed a denser differentiated melanocytic infiltrate in lCMN than in mCMN. Melan-A^+ cells counting showed a 4-fold increase in lCMN compared to mCMN in the dermis (Fig. 1a; lCMN mean ± SEM: 57.35 ± 2.26%; mCMN mean ± SEM: 15.66 ± 0.93%; ***$p \leq 0.001$). $MITF^+$ cells counting revealed a 2-fold increase in lCMN compared to mCMN in the epidermis (Fig. 1b; lCMN mean ± SEM: 14.84 ± 1.21%; mCMN mean ± SEM: 6.8 ± 0.64%; ***$p \leq 0.001$). Both

types of CMN harbored HMB45$^+$ cells, but in lCMN, these cells were predominantly found in the epidermis with a statistically significant increase (Figure S1a).

Sox10 is expressed both by melanocytic precursors and differentiated nevocytes (22). A significantly lower number of Sox10$^+$ cells was found in mCMN in both epidermis and dermis (Fig. 1c). In the dermis, Sox10 was expressed as much as 3 times more in lCMN than in mCMN (Fig. 1c; lCMN mean ± SEM: 6.96 ± 0.90%; mCMN mean ± SEM: 2.27 ± 0.30%; ***$p \leq 0.001$). Stem cell/progenitor marker Nestin (23) and embryonic stem cell transcription factor Oct4 (24) showed a higher expression in lCMN than in mCMN in both epidermis and dermis (Fig. 1d and Fig. 1e respectively). A 5-fold increase of Oct4 expression was observed in both epidermis and dermis of lCMN compared to mCMN (Fig. 1e; lCMN mean ± SEM: 35.57 ± 1.72%; mCMN mean ± SEM: 7.67 ± 0.85%; ***$p \leq 0.001$). Expression of CD44, which is reported both in benign and malignant melanocytic lesions (25), was increased in the dermis of lCMN compared to mCMN (Figure S1b). Finally, Ki67-labeled proliferating cells were strikingly more numerous in lCMN then in mCMN (Fig. 1f). A 4-fold and a 20-fold increase in the number of positive cells were observed in the epidermis and dermis of lCMN respectively compared to mCMN (Fig. 1f; lCMN mean ± SEM: 4.28 ± 0.70%; mCMN mean ± SEM: 0.21 ± 0.1%; ***$p \leq 0.001$).

Altogether, these results confirm the presence within CMN of cells expressing various stem cell and progenitor markers, but at a significantly lower density in mCMN than in lCMN.

Varying *in vitro* clonogenic and proliferative properties according to CMN size

In vitro characteristics of spheroid colonies obtained from mCMN were ascertained through sphere-forming and clonogenic assays. Both mCMN and lCMN cell suspensions gave rise to spheroid colonies (Fig. 2). After 7 and 13 days of culture (DIV7 and DIV13), mCMN colonies' number and size were significantly lower than lCMN colonies' (Fig. 2a).

In order to assert clonogenic abilities of CMN spheres, these colonies were enzymatically dissociated on DIV13. Single cells were replated *de novo* (Figure S2a) and studied over 4 passages (Fig. 2b). As lCMN cells, mCMN cells constantly formed spheres after each passage although their number and diameter was statistically lower (Fig. 2b).

The percentage of mCMN cells giving rise to colonies was calculated using an *in vitro* limiting dilution assay (16,21). The frequencies of colonies initiating cells were 1 in 1540 cells on DIV7 and 1 in 1176 cells on DIV13 (Fig. 2c) and were therefore less frequent then in lCMN (1 in 396 cells on DIV7, *$p \leq 0.05$; 1 in 307 cells on DIV13, **$p \leq 0.01$; Figure S2b). Nevospheres originating from mCMN expressed Melan-A and Oct4 (Figure S3a).

These data support the existence of a clonogenic cell population in mCMN but at a lower frequency than in lCMN.

Varying tumorigenic potential according to CMN size

Finally, the tumorigenic potential of mCMN cells was assessed through xenotransplantation experiments in $Rag2^{-/-}$ immunocompromised mice. Standardized full-thickness CMN specimens were grafted and harvested 3 and 7 months post-transplantation (Fig. 3). A total of 17 specimens from 7 different medium M1 CMN were grafted, 15 of which were harvested and included in the final analysis. A total of 9 specimens from 4 different large/giant CMN were also grafted, 8 of which were harvested and included in the final analysis. After 3 months, there was no statistically significant difference between CMN xenografts regardless of their group and initial punch biopsies. Seven months post grafting, when compared to the original biopsies, mCMN tissues had not statistically significantly increased; conversely, a 3-fold increase was observed in lCMN xenografts compared to mCMN (Fig. 3a). Nevertheless, hematoxylin-eosin staining revealed that both mCMN and lCMN xenografts displayed the same architecture as the original grafted CMN tissues (Fig. 3b, Figure S3a) with a pigmented

outgrowth tissue surrounding a cystic structure as previously reported (Figure S3b). Nuclei counterstained with haematoxylin revealed a higher density of cells in lCMN (Figure S3c). Stainings using anti-human mitochondria antibody were performed in order to confirm that the expanding xenografts were still predominantly composed of human cells and to rule out a possible participation of a murine cell contingent in grafts expansion (Fig. 3b, Figure S4). A human lCMN (Figure S4a) and mouse skin (Figure S4b) were used as positive and negative controls respectively. Immunostainings confirmed that xenografts were still totally of human origin 7 months post-grafting (Fig. 3b areas 1 and 2).

DISCUSSION

Our study has questioned the mechanisms of CMN diversity. We compared post-natal nevocytic cells with clonogenic properties in two categories of *NRAS*-mutated nevi: medium M1 and large/giant CMN. Of note, in order to compare groups as homogeneous as possible, we chose to explore subcategories of CMN; small and medium M2 nevi were therefore excluded from our study. All 28 nevi were *NRAS*-mutated. *BRAF* mutational status was also explored using two different state-of-the-art genotyping technics (18–20). Pyrosequencing has an *NRAS* and *BRAF* mutation detection sensitivity of approximately 7%. Therefore, in order to fully address the question of a possible double *NRAS* and *BRAF* mutation within a specific specimen, we also genotyped nevi using E-*ice*-COLD-PCR, a powerful tool to detect and identify mutations of low abundance. Indeed, E-*ice*-COLD-PCR has an *NRAS* and *BRAF* mutation detection sensitivity of 0.01% to 0.5-1% (9). Nevertheless, we were not able to detect a *BRAF* mutation in any of the 28 *NRAS*-mutated nevi.

In vivo, our immunohistochemistry experiments have shown that both mCMN and lCMN are heterogeneous tissues containing cells expressing various progenitor/stemness markers of the skin and skin tumors. As expected, a significantly lower density of these markers was observed in mCMN than in lCMN. To date, even if the cell of origin has not been clearly identified, our data and others (16,26) support the hypothesis that CMN could originate from one of the identified cutaneous stem cell population.

Analyses of mCMN nevospheres yielded consistent data with what we previously published in the case of lCMN (16). Comparable results have also been obtained by Basu and colleagues in their study of four cases of neurocutaneous melanocytosis (17). They reported the presence of clonogenic cells, capable of forming nevospheres and with similar proliferative and self-renewing abilities. As we observed with CMN cells, a defined set of growth factors was absolutely required for NCM cells' survival and proliferation (17). We showed that, although

cells with particular clonogenic and proliferative potential persisted postnatally in both mCMN and lCMN, their number was significantly lower in mCMN. Indeed, quantitative analysis of *in vitro* limiting dilution assays revealed a four to five-fold statistically significant decrease in the number of colony-initiating cells in mCMN compared to lCMN. We were not able to evaluate initiating cells in a large panel of cases of small and medium M2 nevi in order to definitely correlate the amount of clonogenic cells and nevus size. Nevertheless, the striking difference found between mCMN and lCMN suggests that the initiating cell number may determine PAS in CMN.

A relevant concern is whether our two groups are sufficiently comparable and whether an age disparity might bias our results as newborn and adolescent tissues can present strikingly different characteristics in terms of homeostasis and wound healing. Indeed, the mean age of lCMN and mCMN patients was of 19.5 months (3 months to 5 years) and 45 months (5 months to 16 years) respectively. Age variation was most important in our mCMN group. Xenografts were performed using specimens from 7 different donors of various ages (8 months to 16 years). However, these mCMN xenografts all showed a similar pattern of expansion regardless of donor ages. Similarly, the 3 patients whose mCMN were used for *in vitro* limiting dilution assays had different ages (5 months to 12 years). Nevertheless, the results were extremely reproducible as shown by SEM bars in Fig. 2c.

Our various experiments revealed varying proliferative, clonogenic and tumorigenic potential in the two categories of nevi. This raises the hypothesis of larger pools of stem-like cells being present and persisting post-natally in the larger lesions, which could explain a higher risk of melanoma transformation as a consequence of a second somatic event occurring during life. A recent study supports this hypothesis. Shain et al.(27) have studied the succession of genetic alterations during melanoma progression, comparing individual primary melanomas with their precursor lesions at distinct pathological levels (both benign and intermediate

precursor lesions were analyzed). The authors have reported that precursor lesions (acquired nevi) were initiated by MAPK pathway mutations, namely *BRAF* mutations. Progression was associated with additional driver mutations arising in a specific chronological sequence: *NRAS* and *TERT* promoter mutations (early occurrence), and *CDKN2A* biallelic inactivation, *PTEN* and *TP53* mutations (late occurrence).

Our findings also open an intriguing question about the pathogenesis of CMN. Indeed, all mCMN and lCMN in this study bore an *NRAS* Q61 mutation. Using next generation sequencing, we reported this mutation to be the sole post-zygotic somatic mutation in lCMN (9). The same may hold true for mCMN but has yet to be proved. Etchevers recently raised a very interesting hypothesis based on mice models data to try and explain CMN size and mutational status diversity: smaller lesions could arise from daughter cells deriving from one single somatically mutated cell, where the *NRAS* or *BRAF* driver mutation occurred later than in the larger lesions. As early heterozygous activating *BRAF* mutations are usually incompatible with postnatal survival conversely to *NRAS* mutations, this might explain the difference in CMN mutational status according to size (28).

Nevertheless, our results raise the question of other events leading to *NRAS*-mutated nevi of different sizes with a varying transformation risk. Indeed, germ-line alterations of Wnt signaling have recently been reported in association with somatic *NRAS* activation in lCMN (29). Further addressing this interesting issue would request the performance of other analyses and more specifically a study of epigenetics in mCMN versus lCMN. Lastly, the question about a possible link between this varying clonogenic and tumorigenic potential and the difference reported in terms of malignant degenerescence in small/medium and large/giant CMN remains to be answered.

ACKNOWLEDGMENTS

We are grateful to all the patients and families who participated in this study. We thank Dr Dany Nassar for helpful discussions. We thank Aude Fert, Michèle Oster, Tatiana Ledent and Delphine Muller and the Saint-Antoine Research Center Animal Facility for their technical support. This work was funded by the Société Française de Dermatologie and the Société de Recherche Dermatologique. C.C. was supported by the Fondation René Touraine, Lebanese CNRS and AREMPH.

AUTHORS' CONTRIBUTIONS

Study conception and design: SG, SA. Acquisition of data: SG, NK, AP, TR, CC, ACL, AHK, SF, RF. Analysis and interpretation of data: SG, NK, TR, SA, RF. Drafting and/or critical revision of manuscript: SG, SA, RF. All authors have read and approved the last version of the manuscript.

CONFLICT OF INTEREST

The authors declare no conflict of interest.

SUPPORTING INFORMATION

Additional supporting data may be found in the supplementary information of this article.

Supplementary Methods.

Table S1. Clinical features and nevus categorization.

Figure S1. Human CMN display cells with progenitor/stem cell markers *in vivo*.

Figure S2. *In vitro* human CMN cells characteristics.

Figure S3. Histology of xenografts 7 months postgrafting.

Figure S4. Anti-Human mitochondria immunostainings on human lCMN and mouse skin.

REFERENCES

1 Krengel S, Scope A, Dusza S W *et al.* New recommendations for the categorization of cutaneous features of congenital melanocytic nevi. J Am Acad Dermatol 2013: **68**: 441–451.

2 Kanada K N, Merin M R, Munden A *et al.* A prospective study of cutaneous findings in newborns in the United States: correlation with race, ethnicity, and gestational status using updated classification and nomenclature. J Pediatr 2012: **161**: 240–245.

3 Arons M S, Hurwitz S. Congenital nevocellular nevus: a review of the treatment controversy and a report of 46 cases. Plast Reconstr Surg 1983: **72**: 355–365.

4 Castilla E E, Graça Dutra M da, Orioli-Parreiras I M. Epidemiology of congenital pigmented naevi: I. Incidence rates and relative frequencies. Br J Dermatol 1981: **104**: 307–315.

5 Rhodes A R. Congenital nevomelanocytic nevi. Histologic patterns in the first year of life and evolution during childhood. Arch Dermatol 1986: **122**: 1257–1262.

6 Price H N, Schaffer J V. Congenital melanocytic nevi-when to worry and how to treat: Facts and controversies. Clin Dermatol 2010: **28**: 293–302.

7 Bauer J, Curtin J A, Pinkel D *et al.* Congenital melanocytic nevi frequently harbor NRAS mutations but no BRAF mutations. J Invest Dermatol 2007: **127**: 179–182.

8 Kinsler V A, Thomas A C, Ishida M *et al.* Multiple Congenital Melanocytic Nevi and Neurocutaneous Melanosis Are Caused by Postzygotic Mutations in Codon 61 of NRAS. J Invest Dermatol 2013:

9 Charbel C, Fontaine R H, Malouf G G *et al.* NRAS mutation is the sole recurrent somatic mutation in large congenital melanocytic nevi. J Invest Dermatol 2014: **134**: 1067–1074.

10 Grichnik J M, Ross A L, Schneider S L *et al.* How, and from which cell sources, do nevi really develop? Exp Dermatol 2014: **23**: 310–313.

11 Ichii-Nakato N, Takata M, Takayanagi S *et al.* High frequency of BRAFV600E mutation in acquired nevi and small congenital nevi, but low frequency of mutation in medium-sized congenital nevi. J Invest Dermatol 2006: **126**: 2111–2118.

12 Salgado C M, Basu D, Nikiforova M *et al.* BRAF mutations are also associated with neurocutaneous melanocytosis and large/giant congenital melanocytic nevi. Pediatr Dev Pathol Off J Soc Pediatr Pathol Paediatr Pathol Soc 2015: **18**: 1–9.

13 Kinsler V A, Abu-Amero S, Budd P *et al.* Germline melanocortin-1-receptor genotype is associated with severity of cutaneous phenotype in congenital melanocytic nevi: a role for MC1R in human fetal development. J Invest Dermatol 2012: **132**: 2026–2032.

14 Krengel S, Hauschild A, Schäfer T. Melanoma risk in congenital melanocytic naevi: a systematic review. Br J Dermatol 2006: **155**: 1–8.

15 Vourc'h-Jourdain M, Martin L, Barbarot S *et al.* Large congenital melanocytic nevi: therapeutic management and melanoma risk: a systematic review. J Am Acad Dermatol 2013: **68**: 493–498.e1–14.

16 Charbel C, Fontaine R H, Kadlub N *et al.* Clonogenic cell subpopulations maintain congenital melanocytic nevi. J Invest Dermatol 2015: **135**: 824–833.

17 Basu D, Salgado C M, Bauer B S *et al.* Nevospheres from neurocutaneous melanocytosis cells show reduced viability when treated with specific inhibitors of NRAS signaling pathway. Neuro-Oncol 2015:

18 How-Kit A, Lebbé C, Bousard A *et al.* Ultrasensitive detection and identification of BRAF V600 mutations in fresh frozen, FFPE, and plasma samples of melanoma patients by E-ice-COLD-PCR. Anal Bioanal Chem 2014: **406**: 5513–5520.

19 How Kit A, Mazaleyrat N, Daunay A *et al.* Sensitive detection of KRAS mutations using enhanced-ice-COLD-PCR mutation enrichment and direct sequence identification. Hum Mutat 2013: **34**: 1568–1580.

20 How-Kit A, Tost J. Pyrosequencing®-Based Identification of Low-Frequency Mutations Enriched Through Enhanced-ice-COLD-PCR. Methods Mol Biol Clifton NJ 2015: **1315**: 83–101.

21 Liu M, Miller C L, Eaves C J. Human long-term culture initiating cell assay. Methods Mol Biol Clifton NJ 2013: **946**: 241–256.

22 Sommer L. Generation of melanocytes from neural crest cells. Pigment Cell Melanoma Res 2011: **24**: 411–421.

23 Sharma B K, Manglik V, Elias E G. Immuno-expression of human melanoma stem cell markers in tissues at different stages of the disease. J Surg Res 2010: **163**: e11–15.

24 Cheli Y, Giuliano S, Guiliano S *et al.* Mitf is the key molecular switch between mouse or human melanoma initiating cells and their differentiated progeny. Oncogene 2011: **30**: 2307–2318.

25 Leigh C J, Palechek P L, Knutson J R *et al.* CD44 expression in benign and malignant nevomelanocytic lesions. Hum Pathol 1996: **27**: 1288–1294.

26 Kinsler V A, Anderson G, Latimer B *et al.* Immunohistochemical and ultrastructural features of congenital melanocytic naevus cells support a stem-cell phenotype. Br J Dermatol 2013: **169**: 374–383.

27 Shain A H, Yeh I, Kovalyshyn I *et al.* The Genetic Evolution of Melanoma from Precursor Lesions. N Engl J Med 2015: **373**: 1926–1936.

28 Etchevers H C. Hiding in plain sight: molecular genetics applied to giant congenital melanocytic nevi. J Invest Dermatol 2014: **134**: 879–882.

29 Pawlikowski J S, Brock C, Chen S-C *et al.* Acute Inhibition of MEK Suppresses Congenital Melanocytic Nevus Syndrome in a Murine Model Driven by Activated NRAS and Wnt Signaling. J Invest Dermatol 2015:

TABLES

Table 1. Clinical and genetic characteristics of the 18 medium M1 and 10 large/giant CMN[a]

Patient	Age	Sex	Body site	PAS (cm)	Krengel classification	BRAF* Sequencing	NRAS* Sequencing	Experiments
1	13mo	M	Trunk	1.5-10	Medium M1	WT	NRAS3 Q61K	IL, spheres
2	6y	F	Leg	1.5-10	Medium M1	WT	NRAS3 Q61K	IL
3	8mo	F	Trunk	1.5-10	Medium M1	WT	NRAS3 Q61K	IL, xenografts
4	16mo	F	Head	1.5-10	Medium M1	WT	NRAS3 Q61R	IL
5	33mo	M	Leg	1.5-10	Medium M1	WT	NRAS3 Q61R	IL
6	22mo	M	Leg	1.5-10	Medium M1	WT	NRAS3 Q61K	IL
7	3.5y	M	Trunk	1.5-10	Medium M1	WT	NRAS3 Q61K	Xenografts
8	16y	F	Leg	1.5-10	Medium M1	WT	NRAS3 Q61K	Xenografts
9	3y	M	Head	1.5-10	Medium M1	WT	NRAS3 Q61R	Xenografts
10	14mo	F	Head	1.5-10	Medium M1	WT	NRAS3 Q61R	Xenografts
11	6y	F	Arm	1.5-10	Medium M1	WT	NRAS3 Q61K	Xenografts
12	3y	F	Arm	1.5-10	Medium M1	WT	NRAS3 Q61K	Xenografts
13	5mo	M	Trunk	1.5-10	Medium M1	WT	NRAS3 Q61K	Spheres
14	17mo	M	Head	1.5-10	Medium M1	WT	NRAS3 Q61K	Spheres
15	6.5y	M	Trunk	1.5-10	Medium M1	WT	NRAS3 Q61K	Spheres
16	12mo	M	Trunk	1.5-10	Medium M1	WT	NRAS3 Q61R	LDA, spheres
17	12y	F	Trunk	1.5-10	Medium M1	WT	NRAS3 Q61K	LDA, spheres
18	5mo	F	Face	1.5-10	Medium M1	WT	NRAS3 Q61R	LDA
19	3.5y	F	Head	>20-30	Large L1	WT	NRAS3 Q61K	IL
20	5y	F	Arm	>20-30	Large L1	WT	NRAS3 Q61R	IL
21	7mo	M	Trunk	>40-50	Giant G1	WT	NRAS3 Q61R	LDA, spheres, xenogafts, IL
22	4mo	F	Trunk	>20-30	Large L1	WT	NRAS3 Q61K	Spheres, xenografts, IL
23	9mo	F	Head	>20-30	Large L1	WT	NRAS3 Q61R	Xenografts, IL
24	3mo	M	Head	>20-30	Large L1	WT	NRAS3 Q61K	Spheres, xenografts
25	5mo	M	Head	>20-30	Large L1	WT	NRAS3 Q61K	Spheres
26	4mo	F	Head	>20-30	Large L1	WT	NRAS3 Q61K	LDA, spheres
27	13mo	F	Trunk	>30-40	Large L2	WT	NRAS3 Q61R	Spheres
28	4y	M	Arm	>20-30	Large L1	WT	NRAS3 Q61K	LDA, spheres

[a]Abbreviations: mo, month; y, year; M, male; F, female; WT, wild type; IL, immunolabeling; LDA, limiting dilution assay.

* Pyrosequencing was used to screen *NRAS* exon 2 and 3 and *BRAF* exon 15 mutations. Mutation enrichment by Enhanced-ice-COLD-PCR was also used to screen *BRAF* exon 15 and *NRAS* exon 3 mutations.

FIGURE LEGENDS

Figure 1. Human CMN display cells with progenitor/stem cells markers.

Number of positive cells per total cells in epidermis and dermis of human medium M1 (mCMN n=5) and large Congenital Melanocytic Nevi (lCMN n=5) after staining for Melan-A (a), MITF (b), Sox10 (c), Nestin (d), Oct4 (e) and Ki67 (f). $MITF^+$, $Nestin^+$, $Ki67^+$ cells were stained with AEC chromogen. $Melan\text{-}A^+$ and $Sox10^+$ cells were stained with Alexa488-conjugated antibodies; $Oct4^+$ cells with Cy3-conjugated antibodies. Dotted line separates dermis from epidermis. Scale bar = 100 µm. * represents difference between mCMN and lCMN. *p≤0.05, ***p≤0.001 in Student's t-test.

Figure 2. Human CMN cells display varying *in vitro* clonogenic and proliferative properties according to CMN size.

(a) Sphere formation assay. Photomicrographs (left panel) and histograms (right panel) of mCMN (n=3) and lCMN (n=4) colonies on DIV7 and DIV13 with number and diameter of colonies. Scale bar = 100 µm. * represents difference between mCMN and lCMN. **p≤0.01, ***p≤0.001 in Student's t-test.

(b) Cell passages. Diameter of colonies of mCMN and lCMN colonies on DIV13 after 4 passages (mCMN n=3; lCMN n=3). * represents difference between mCMN and lCMN. *p≤0.05, ***p≤0.001 in Student's t-test.

(c) Limiting dilution assays. mCMN cells were plated with decreasing concentrations from 2000 to 10 cells/well. Colonies numbers were counted on DIV7 and 13. 1/1540 and 1/1176 initiating cells were capable of forming colonies on DIV7 and DIV13 respectively (SEM bars are represented).

Figure 3. *In vivo* xenotransplantation of CMN tissue in immunocompromised mice

Standardized biopsies of mCMN and lCMN were grafted in Rag2$^{-/-}$ mice and collected after 3 or 7 months (mCMN n=15; lCMN n=8 grafted specimens). (**a**) Three-fold expansion of the lCMN xenografts after 7 months when compared to mCMN xenografts. Scale bar = 2 mm. **p≤0.01 in Student's t-test. (**b**) Histology of mCMN and lCMN whole graft tissue 7 months postgrafting. Scale bar = 250 µm. (1) and (2) are close up views of the lCMN xenograft after immunolabeling using an anti-human mitochondria Cyanine3-conjugated antibody showing the human origin of cells. Scale bar = 50 µm.

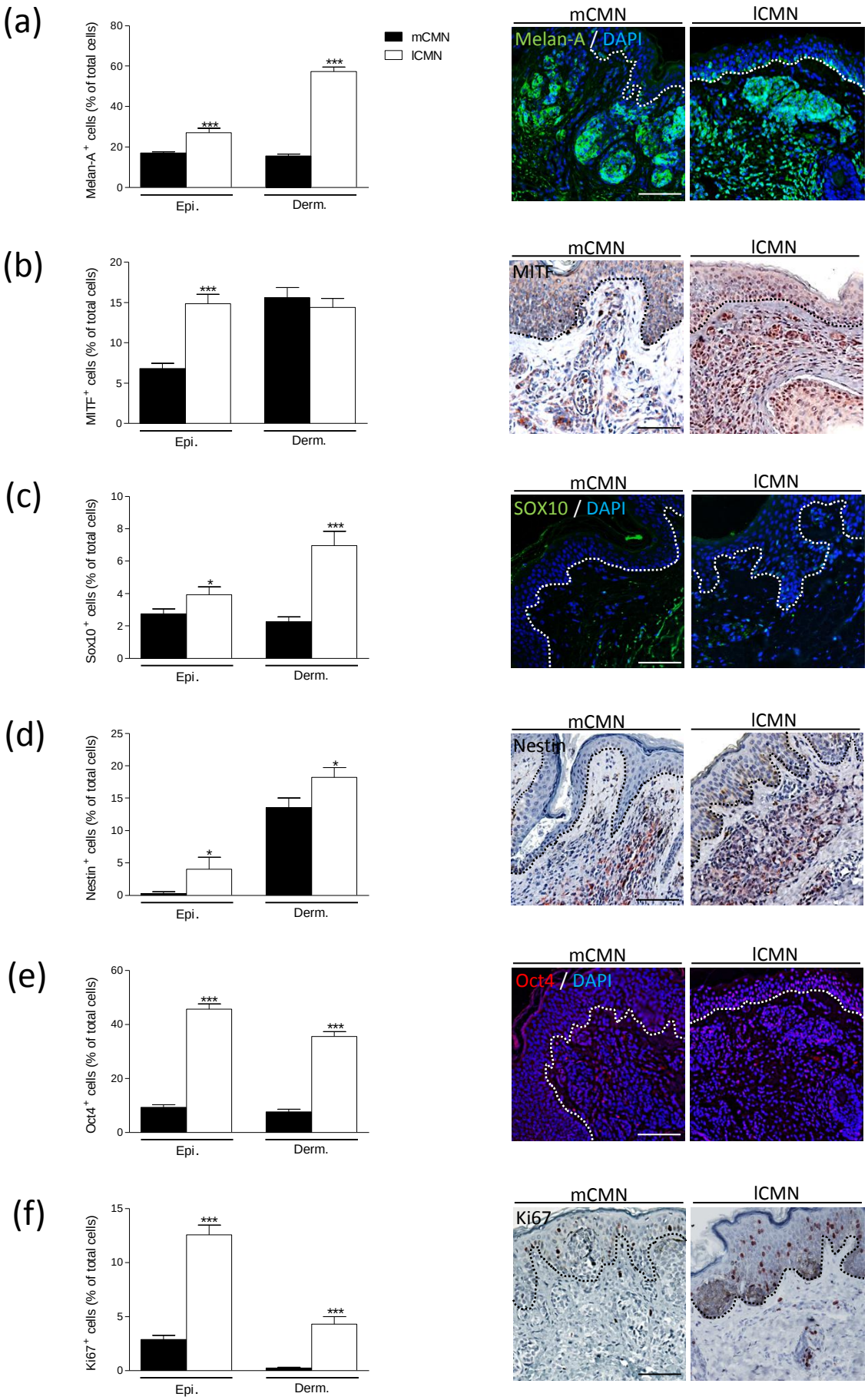
(a)
Melan-A+ cells (% of total cells)
mCMN
lCMN
Epi.
Derm.
mCMN
lCMN
Melan-A / DAPI
(b)
MITF+ cells (% of total cells)
Epi.
Derm.
mCMN
lCMN
MITF
(c)
Sox10+ cells (% of total cells)
Epi.
Derm.
mCMN
lCMN
SOX10 / DAPI
(d)
Nestin+ cells (% of total cells)
Epi.
Derm.
mCMN
lCMN
Nestin
(e)
Oct4+ cells (% of total cells)
Epi.
Derm.
mCMN
lCMN
Oct4 / DAPI
(f)
Ki67+ cells (% of total cells)
Epi.
Derm.
mCMN
lCMN
Ki67

Figure 2.

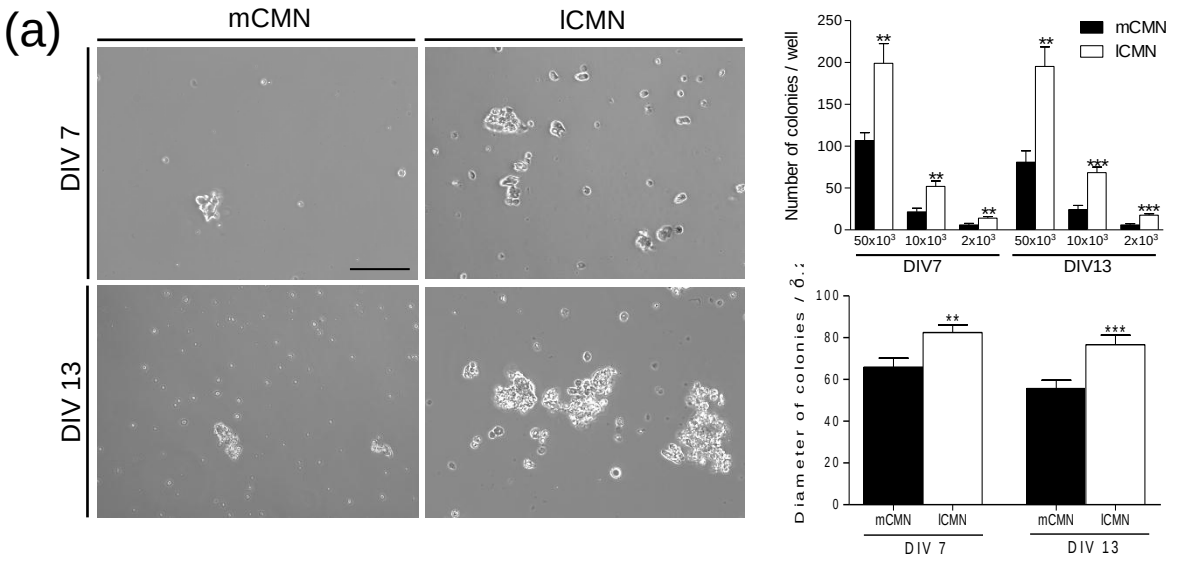
(a)
mCMN
lCMN
DIV 7
DIV 13
Number of colonies / well
mCMN
lCMN
50x10³
10x10³
2x10³
DIV7
DIV13
Diameter of colonies / d.
mCMN
lCMN
DIV 7
DIV 13

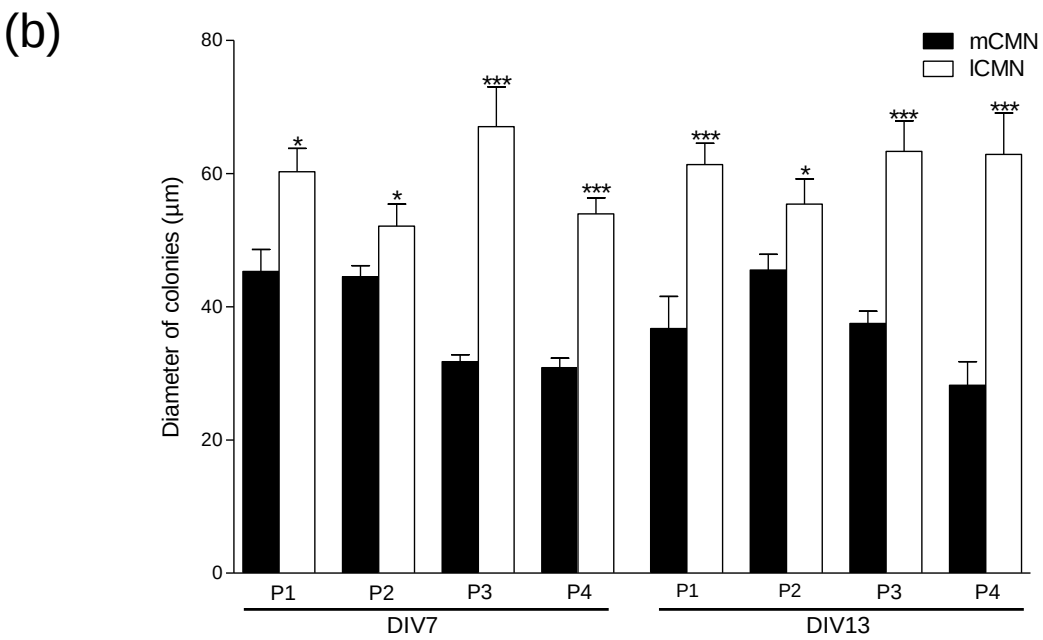
(b)
mCMN
lCMN
Diameter of colonies (µm)
P1
P2
P3
P4
DIV7
DIV13

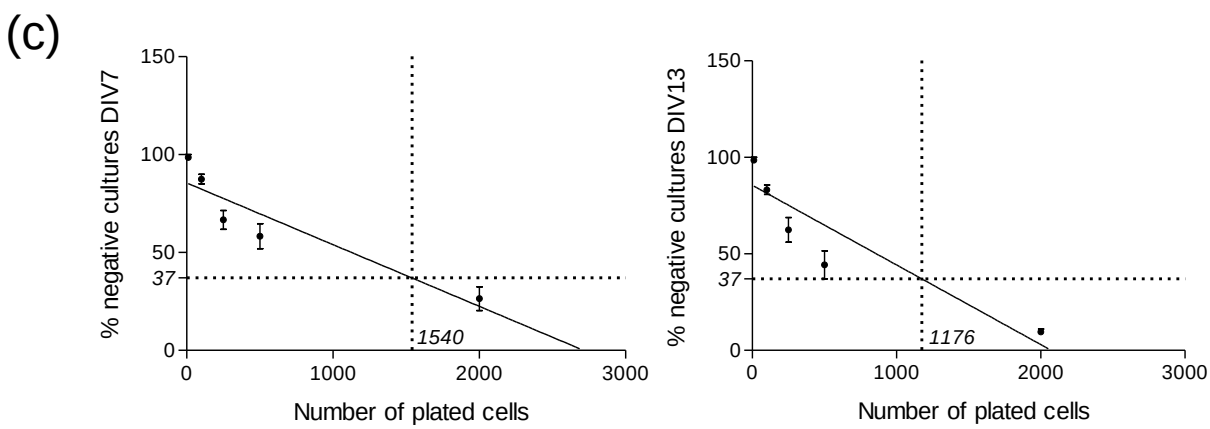
(c)
% negative cultures DIV7
Number of plated cells
1540
% negative cultures DIV13
Number of plated cells
1176

Figure 3.

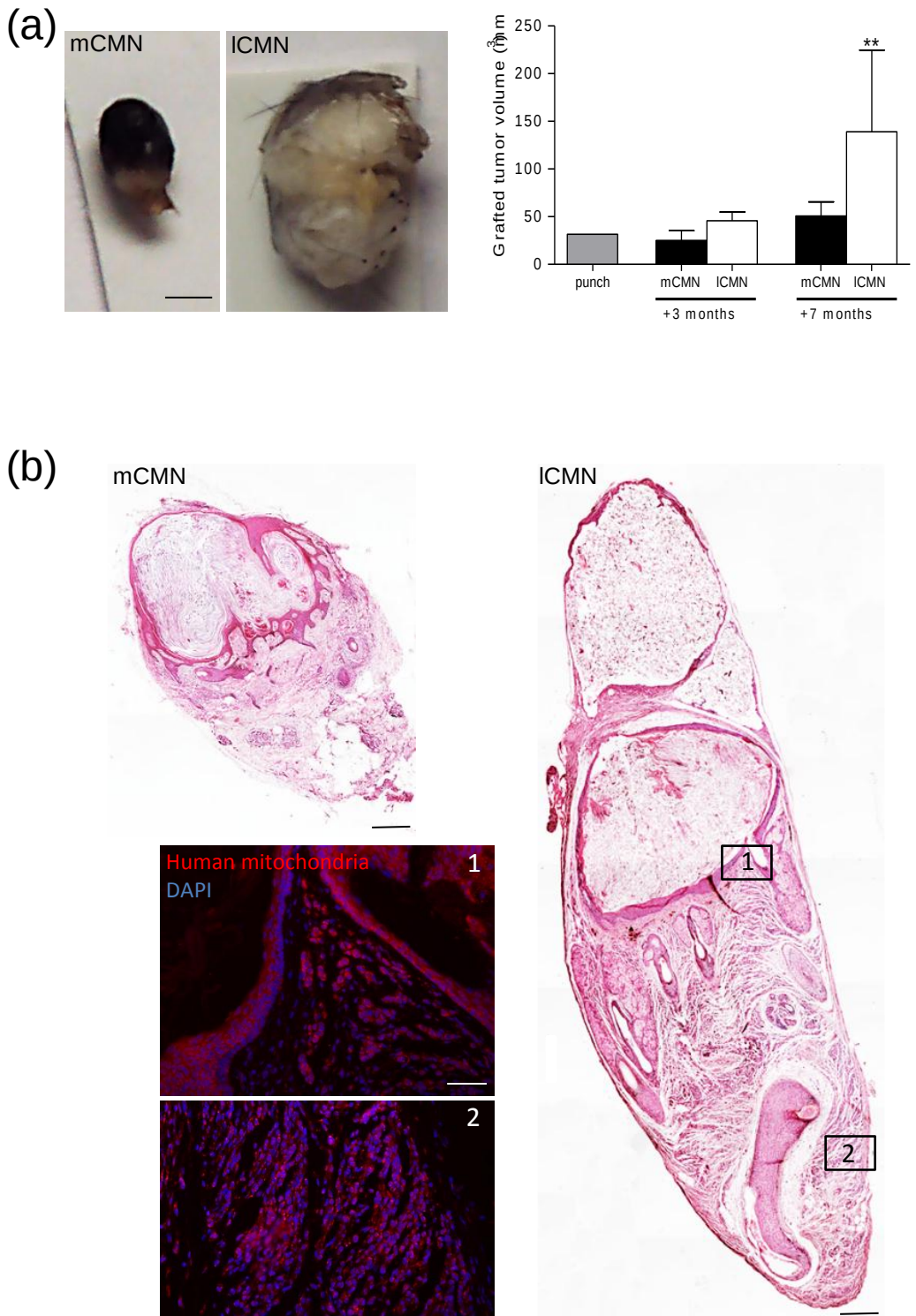
(a)
mCMN
lCMN
Grafted tumor volume (mm3)
250
200
150
100
50
0
**
punch
mCMN
lCMN
mCMN
lCMN
+3 months
+7 months
(b)
mCMN
lCMN
Human mitochondria
DAPI
1
2
1
2

SUPPLEMENTARY DATA

Supplementary Methods

Immunostainings

Formalin-fixed paraffin-embedded CMN tissue sections (5 µm) were obtained from the department of Pathology at Trousseau Hospital. Tissue sections were labeled with the following antibodies: Rabbit anti-human MITF (dilution 1:250, ab20663, Abcam, Cambridge, UK), mouse anti-human Nestin (dilution 1:100, ab22035, Abcam), mouse anti-human HMB45 (pre-diluted, ab51935, Abcam), mouse anti-human KI67 (dilution 1:100, NCL-L-Ki67-MM1, Novocastra, Wetzlar, Germany), rabbit anti-human CD44 (dilution 1:100, ab51037, Abcam), rabbit anti-human Oct4 (dilution 1:100, ab19857, Abcam), mouse anti-human Melan-A (dilution 1:100, ab3168, Abcam) and rabbit anti-human Sox10 (dilution 1:100, sc-17342, Santa Cruz Biotechnology, Santa Cruz, CA, USA).

Antigen retrieval was performed by incubating the slides with citrate buffer (pH=6) or EDTA buffer (pH=9) at 98°C for 20 min. Non specific antigen sites were blocked in PBS with 3% BSA with 10 or 20 % serum goat.

For MITF, Nestin, Ki67, CD44 and HMB45 stainings, endogenous peroxidase activity was blocked with 3 % H2O2 for 10 min. The sections were incubated with the different primary antibodies overnight in PBS with 3% BSA and 0.1% triton for intracellular staining. Staining was achieved using appropriate biotinylated goat anti-mouse or anti-rabbit secondary antibodies (BA9200, BA1000, Vector Laboratories, Burlingame, CA, USA) and Avidine Biotine complex (PK-6100, Vector Laboratories). Bound antibodies were visualized using aminoethylcarbazol (SK-4205, Vector Laboratories) as chromogen. Nuclei were counterstained with Mayer's haematoxylin (TA-125-MH, Thermoscientific, Waltham, MA, USA).

For Melan-A, Sox 10 and Oct-4 immunofluorescence, slides were incubated overnight with primary antibodies diluted with 3% BSA and 0.1% triton for intracellular staining. Sections were washed with PBS followed by secondary antibody goat anti-mouse Alexa 488 (dilution 1:100, A10680, Life Technologies, Carlsbad, CA, USA), or goat anti-rabbit Cy3 (dilution 1:1000, A10522, Life Technologies) for 45 min at room temperature. Slides were also incubated with DAPI (D9542, Sigma-Aldrich, Saint-Louis, MO, USA) for 5 min for nuclei staining and coverslipped using Fluoromount G (0100-01, Southern Biotech, Birmingham, AL, USA).

Negative controls were performed in parallel with the samples substituting the primary antibody with the equivalent isotype.

Photomicrographs were obtained under x20 objective using Nikon Eclipse 90i microscope (Nikon, Tokyo, Japan). Using Image J software, positive cells were counted in 100 µm2 randomized surface squares in both epidermis and dermis of each specimen. In each area, the number of positive cells was counted and reported to the total number of DAPI+ cells. Thus, results are expressed as a percentage of positive cells for each marker analyzed per total cells per 100 mm2 surface areas, both in the epidermis and dermis. Quantitations were done on various parts of the CMN and always in areas within the lesions, usually in the center: these lesions were dissected in a gridded fashion and 3 different sectors were analyzed; for each different sector of the lesions, 3 different areas of 100 µm2 were counted.

In vitro assays

Fresh CMN tissues were manually dissected into small pieces, before sequential enzymatic digestion in Dispase II (2%, 049420780001, Roche, Basel, Switzerland) overnight at 4°C, then in Collagenase I (3.5%, 17100-017, Life Technologies) for 1 hour at 37°C. Cells were filtered using 100 µm and 40 µm cell strainers to obtain a single-cell suspension.

For sphere formation assay, the nevocytic single cell suspension was seeded at a density of 50000 cells/ml in a 12-well plate in DMEM/F12 (31966021-317655027, Life Technologies) supplemented with EGF (100ng/mL, PHG0311, Life Technologies), bFGF (100 ng/mL, PHG0026, Life Technologies), B27 supplement (10889-038, Life Technologies) and insulin (5 ug/mL, I2643-25, Sigma-Aldrich). The number of colonies was counted per well. The diameter was also measured on "day in vitro" DIV7 and DIV13 using Image J software.

For serial passages, the culture medium was collected on DIV13, centrifuged at 500 rpm for 15 min. Spheres were dissociated using pro-accutase (A11105, Life Technologies) 10 min at 37°C, and single cells were seeded again.

The number and frequency of initiating cells was obtained as previously described (16). CMN cells were seeded at ratios of 2000, 500, 250, 100 and 10 cells per well. Using optical microscope (Olympus ULWCD 0.30, Tokyo, Japan), wells containing spheres were counted on DIV7 and 13. The frequency of initiating cells corresponding to 37% of negative wells according to the Poisson statistics was calculated with GraphPad Prism.

Immunocytofluorescence on CMN nevospheres was performed as previously described (16). The following antibodies were used: anti-Melan-A (mouse anti-human, dilution 1:100, Abcam), anti-Oct4 (rabbit anti-human, dilution 1:50, Abcam), as well as anti-mouse Alexa 488 and anti- rabbit Cy3 secondary antibodies.

Supplementary Table 1. Clinical features and nevus categorization[a]

	Medium 1 nevus	Large/giant nevus
Median age[b]	45mo [5mo to 16y]	19.5mo[3mo to 5y]
Female	9/18 (50%)	6/10 (60%)
Nevus site		
Extremities	6/18 (33.3%)	2/10 (20%)
Trunk	7/18 (38.9%)	3/10 (30%)
Head	5/18 (27.8%)	5/10 (50%)
Number of satellites		
S0	16/18 (88.9%)	3/10 (30%)
S1	2/18 (11.1%)	6/10 (60%)
S2	0	1/10 (10%)
S3	0	0
Color heterogeneity		
C0	10/18 (55.6%)	1/10 (10%)
C1	8/18 (44.4%)	4/10 (40%)
C2	0	5/10 (50%)
Surface rugosity		
R0	17/18 (94.4%)	2/10 (20%)
R1	1/18 (5.6%)	4/10 (40%)
R2	0	4/10 (40%)
Dermal or subcutaneaous nodules		
N0	17/18 (94.4%)	6/10 (60%)
N1	1/18 (5.6%)	1/10 (10%)
N2	0	3/10 (30%)
Hypertrichosis		
H0	11/18 (61.1%)	1/10 (10%)
H1	3/18 (16.7%)	2/10 (20%)
H2	4/18 (22.2%)	7/10 (70%)

[a]Data are expressed as *n* (%) unless otherwise indicated ; nevus categorization as described in (1) : S0-S3: grading of nevus satellites; C0-C2: grading of color heterogeneity; R0-R2: grading of nevus rugosity; N0-N2: grading of nodules; H0-H2: grading of hypertrichosis.

[b]Abbreviations : mo, month; y, year.

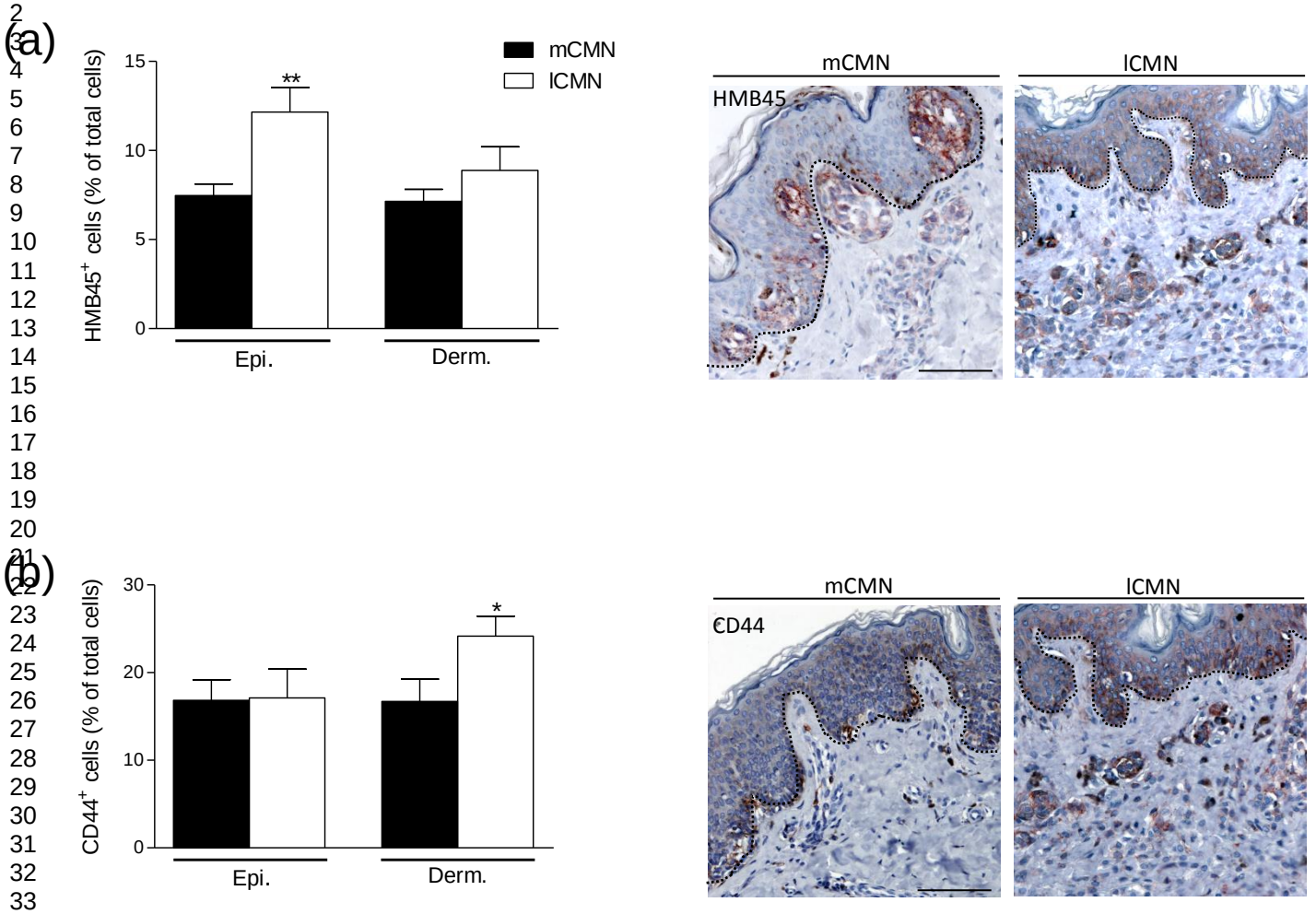

Human CMN display cells with progenitor/stem cell markers *in vivo*.

(a, b) Number of positive cells per total cells in epidermis and dermis of human medium (mCMN n=5) and large Congenital Melanocytic Nevi (lCMN n=5) after staining for HMB45 (a) and CD44 (b) and using AEC chromogen. Dotted line separates dermis from epidermis. * represents the difference between mCMN and lCMN. *p≤0.05, **p≤0.01 in Student's t-test.

Supplementary Figure 2.

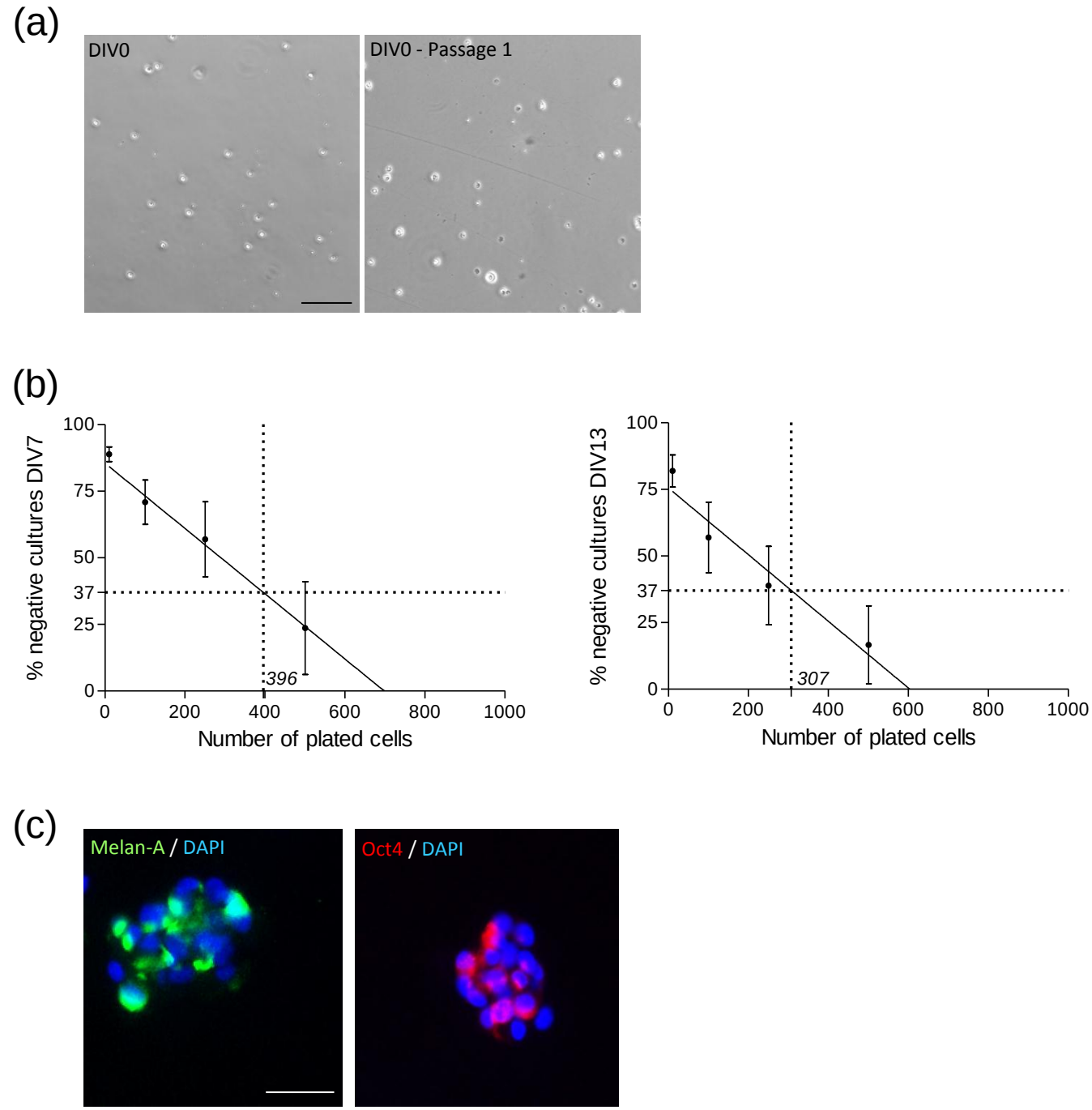

***In vitro* human CMN cells characteristics.**

(a) Photomicrographs showing single plated mCMN cells on DIV0 after tissue dissociation and after passage 1. Scale bar = 100 µm.

(b) Limiting dilution assays of lCMN cells plated at decreasing concentrations from 500 to 10 cells/well. Colonies numbers were counted on DIV7 and 13. 1/396 and 1/307 initiating cells were capable of forming colonies on DIV7 and DIV13 respectively (SEM bars are represented).

(c) Immunocytochemistry of mCMN nevospheres. Melan-A$^+$ (left panel) and Oct4$^+$ (right panel) were stained with Alexa488 and Cy3 secondary antibodies respectively. Scale bar = 50 µm.

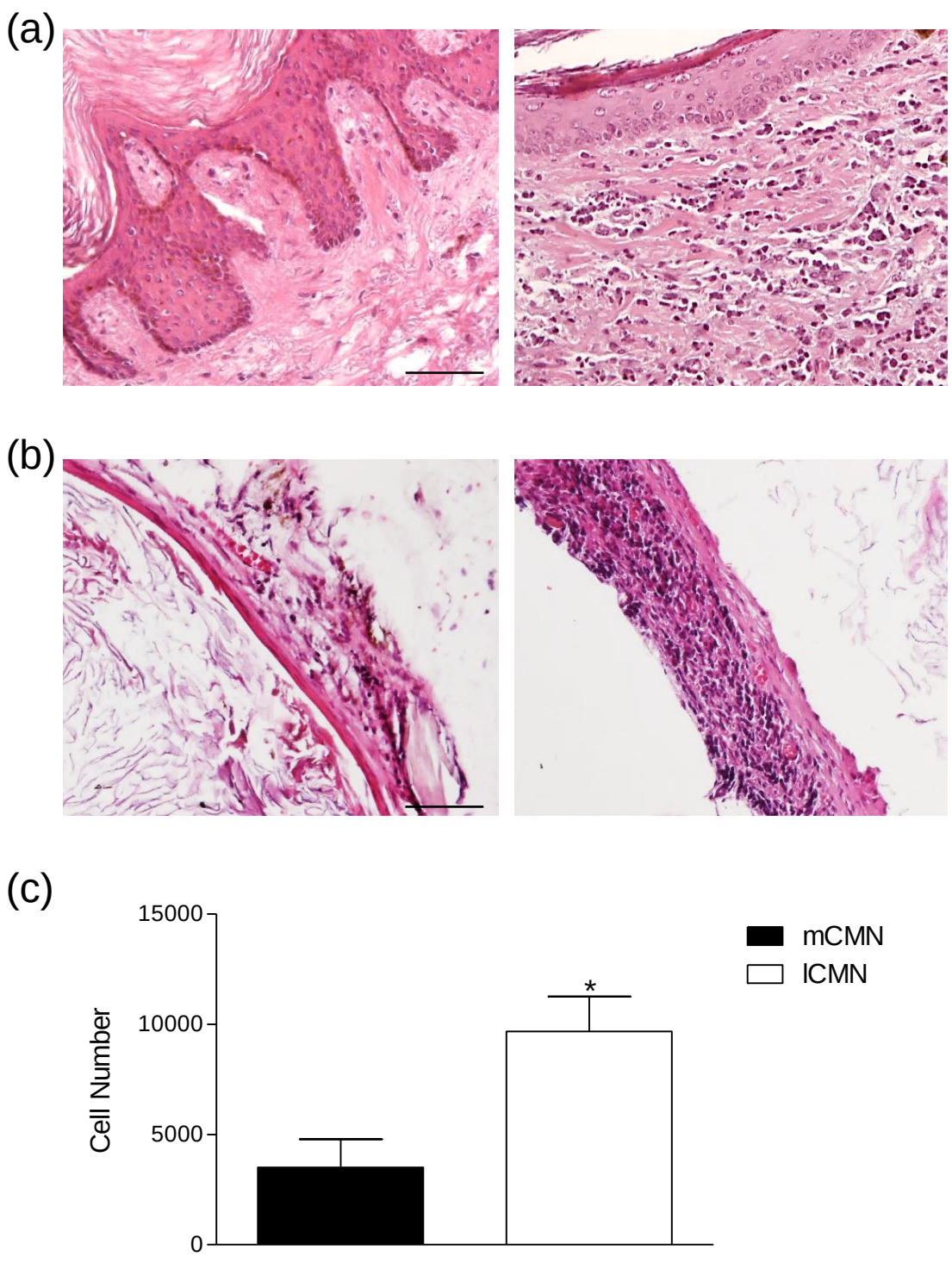

Histology of xenografts 7 months postgrafting.
Both mCMN and lCMN xenografts displayed the same architecture as (a) the original grafted CMN tissues with (b) a surrounding pigmented outgrowth tissue (b). (c) Counting of nuclei counterstained with haematoxylin revealed higher cell numbers in lCMN (n=3) as compared to mCMN (n=3). Scale bar = 100 µm. * represents the difference between mCMN and lCMN. *p≤0.05 in Student's t-test.

Supplementary Figure 4.

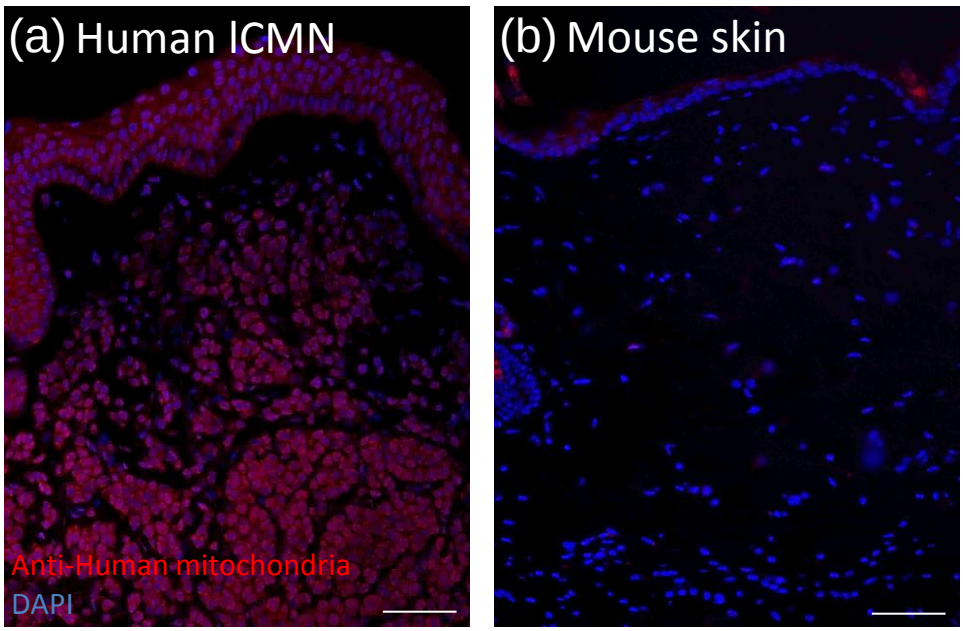

Anti-Human mitochondria immunostainings on human lCMN (a) and mouse skin (b). (a) Human lCMN was used as positive control : all cells were labeled with anti-human mitochondria antibody. (b) Conversely, no cells were labeled when using the same antibody on mouse skin. Scale bar = 50 µm.